Vacuum packaged low-power resonant MEMS strain sensor

Cuong D. Do, Andreja Erbes, Jize Yan, Kenichi Soga and Ashwin A. Seshia

***Abstract*—This paper describes a technical approach towards the realization of a low-power temperature-compensated micromachined resonant strain sensor. The sensor design is based on two identical and orthogonally-oriented resonators where the differential frequency is utilized to provide an output proportional to the applied strain with temperature compensation achieved to first order. Interface circuits comprising of two front-end oscillators, a mixer and low-pass filter are designed and fabricated in a standard 0.35µm CMOS process. The characterized devices demonstrate a scale factor of 2.8Hz/µε over a strain range of 1000µε with excellent linearity over the measurement range. The compensated frequency drift due to temperature is reduced to 4% of the uncompensated value through this scheme. The total continuous power consumption of the strain sensor is 3µW from a 1.2V supply. This low power implementation is essential to enable battery-powered or energy harvesting enabled monitoring applications.**

***Index Terms*—MEMS resonator, Resonant sensor, Oscillator, MEMS-CMOS interface, Temperature compensation**

I. Introduction

DISTRIBUTED wireless sensing is increasingly viewed as an important enabling technology for a range of applications such as structural health monitoring of large-scale built infrastructure [1, 2] and in environmental monitoring [3, 4]. These applications may ultimately require operation in remote, inaccessible locations over lifetimes of several decades where battery replacement is impractical or expensive. This requirement puts a significant constraint on the power demand of the sensors themselves [1, 5, 6]. Silicon micromachined resonant sensors have emerged as a potential candidate to address this requirement [7-11]. They have the inherent potential of being compatible with batch fabrication, miniaturization and can also be co-integrated with CMOS circuitry in a small form-factor package.

Strain gauges are often employed for a variety of structural health monitoring applications and most deployments still rely on foil gauges [12] or piezoresistive strain gauges [13]. Traditional foil gauges and piezoresistive strain gauges are usually associated with significant static power dissipation, both in the transducer element as well as in the associated interface circuitry. While MEMS resonant strain gauges have promised significantly lower power consumption [11] than traditional foil gauges, a low-power implementation has not yet been reported to date.

The use of micromachined flexural resonators as strain sensors has been previously proposed and the early concepts were initially implemented using quartz technology [14, 15]. This was followed by clamped-clamped beam resonators and double-ended tuning fork resonators fabricated using silicon micromachining [16-18]. The device principle is similar to that used for macroscopic vibrating wire strain gauges where in an external axial strain is coupled as a resonant frequency shift in the response. Miniaturization enables significant enhancements in device sensitivity and recent work has demonstrated a strain resolution of better than 4 nε in a 1 Hz bandwidth using board-level interface circuits [9]. The optimization of the power dissipation of these sensors, particularly by implementing the front-end electronics in standard CMOS, has not been previously pursued.

MEMS resonators have also been previously employed as transducers in accelerometers, gyroscopes, strain sensors, electrometers and gravimetric sensors [7, 9, 16-19]. A low power front-end interface circuit [11] for such resonators thus has broad applicability to a variety of sensing contexts. This would enable ultra-low power operation for both the MEMS sensors as well as the interface circuit in order to address practical applications. However, one of the primary challenges for resonant sensors is to distinguish between frequency variations caused by the measurand as opposed to those induced by temperature variations. In the strain gauge application where the sensor is mounted on an external host structure, the variations in temperature can unexpectedly modify the resonator output via two primary effects. First, the material and geometric properties of the resonator are functions of temperature. Secondly, the differential thermal expansion of the materials used in the fabrication of the sensor including the mounting and packaging also induce temperature-dependent axial stress in the resonator in a complex manner [20].

Various techniques such as using a thermometer [21], micro-ovenization [22], multi-layers with different thermal coefficients [23, 24], degenerate-doping [25] and dual-mode [26] approaches have been applied to compensate for temperature effects in MEMS resonators and oscillators. However, in the context of a strain gauge, the above

The authors are with the Department of Engineering, University of Cambridge, Cambridge CB2 1PZ, United Kingdom
Corresponding author: Ashwin A. Seshia (aas41@cam.ac.uk)
This work was supported by the UK Engineering and Physical Sciences Research Council (Grant No. EP/K000314/1).

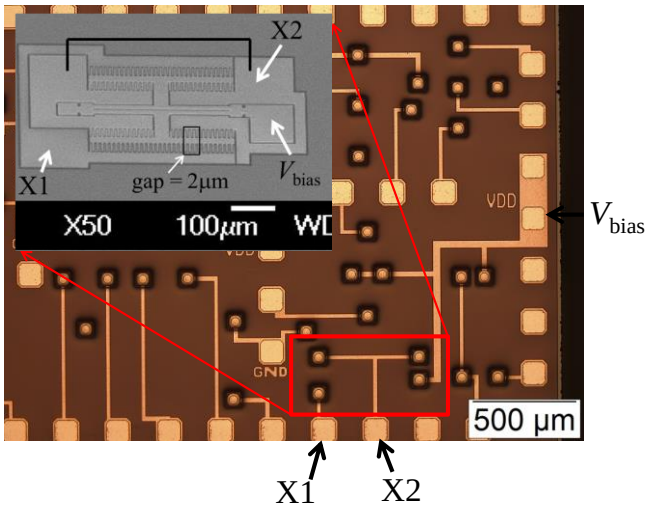

Fig. 1. Top view of the chip-level vacuum packaged silicon die that includes DETF resonator. Inset shows the SEM micrograph of the DETF resonator before encapsulation. The red square shows the location of the tested resonator on the die prototype.

mentioned approaches may not entirely compensate for the stress induced effects [27] on the resonator as these usually address only the variations in material properties and not the variations resulting from the packaging of the sensor to ensure effective and adequate strain transfer from the host structure. Micro-oven control is usually implemented by stabilizing the resonator element at a set point higher than the maximum operating temperature through an integrated heating element. While this could be applied to strain sensors as well, the approach is generally associated with significant power consumption. A common compensation technique incorporating a dummy or un-stressed identical resonator as a reference [20] therefore offers a better alternative for resonator-based strain gauges.

Here, we introduce for the first time, a low-power CMOS-based temperature compensation technique for strain sensors based on vacuum-packaged dual MEMS resonators. This technique incorporates a new low-power circuit topology to resolve the frequency difference between two frequency sources. The device demonstrates a scale factor of 2.8Hz/με over a strain range up to 1000με while consuming 3 microwatts from a 1.2V supply. The fabricated prototype demonstrates a reduction in temperature sensitivity by 96%, from 6.3 Hz/ºC down to 0.2Hz/ºC in the temperature range spanning from 22ºC to 80ºC.

TABLE I
COMB-DRIVE RESONATOR DATA

Parameters	Value
Silicon thickness	30μm
Finger gap spacing	2μm
No. finger X1-beam overlap	64
No. finger X2-beam overlap	56
DETF beam dimensions	300 x 6.5μm
Tine gap	5μm

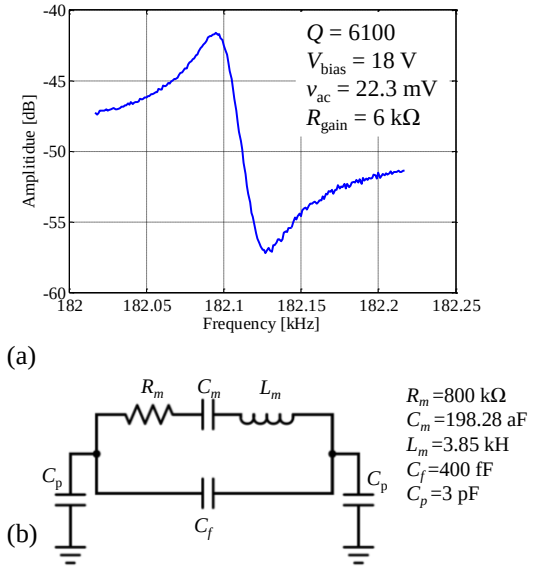

Fig. 2. (a) Open-loop frequency response of the resonator at 18-V bias, f=182.1 kHz, Q = 6100. (b) Electrical equivalent circuit showing extracted device parameters.

II. MEMS RESONATOR

A. Double-Ended Tuning Fork

A comb-drive micro-fabricated double-ended tuning fork (DETF) resonator, Fig. 1, based on previous works [9, 10] is used as the resonant element. The device is designed and fabricated in a foundry process (MIDIS) based on silicon-on-insulator (SOI) wafers and integrated into a wafer-level vacuum package process by Teledyne/DALSA. The operating principle of the DETF resonator is discussed elsewhere [28]. Design parameters of the resonator are summarized in Table I.

The measured quality factor (Q) of the resonator is 6100 and the primary mode resonance frequency (anti-phase mode) at room temperature (~22ºC) and for a V_{bias} = 18V is 182.1kHz. The frequency response is shown in Fig. 2(a). The electrical behaviour of the resonator is similar to that of a series RLC tank [29], Fig. 2(b). The electrical equivalent parameters of the tank circuit are extracted from the measured open-loop data using a two-port network analyzer setup. The parasitic capacitance, C_p, is determined by the device electrode

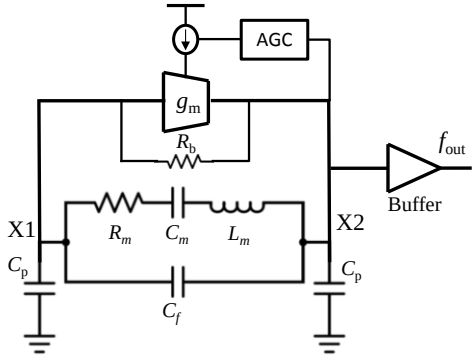

Fig. 3. Block diagram of the Pierce oscillator.

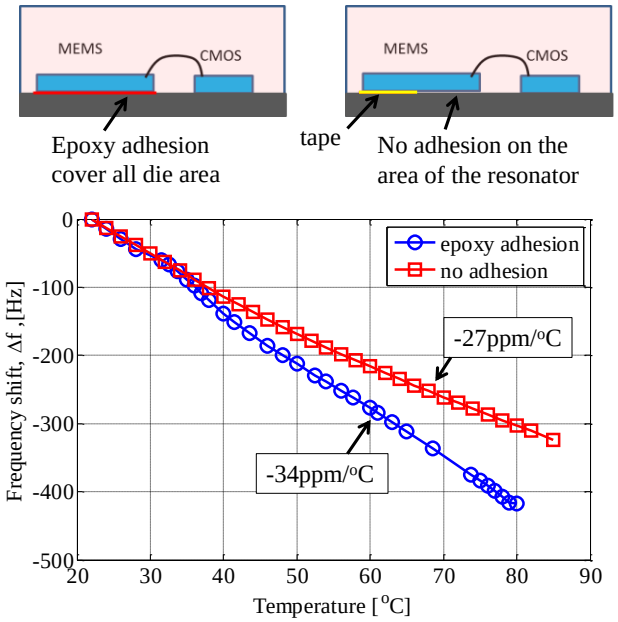

Fig. 4. MEMS resonant frequency shifts with temperature and comparison between epoxy adhesion layer versus no adhesion layer (no adhesion on the area of the resonator) between MEMS die and chip carrier.

geometry and area of interconnects and bondpads.

A high DC bias voltage, V_{bias}, is applied to the resonator body to facilitate transduction of the motional signal with no associated power dissipation [29]. Here, two 9-V batteries connected in series were used to provide this bias voltage. The V_{bias} voltage could be reduced by increasing the transduction area or using a process providing for a reduced package pressure to limit viscous damping and/or smaller minimum actuation gap. For example, if the gap spacing in this process is reduced to 133nm (keeping other resonator parameters constant), the DC bias voltage can be reduced to 1.2V to achieve equivalent performance [29].

A feedback oscillator is constructed as the front-end interface to the DETF resonator. A CMOS circuit based on Pierce topology [11, 30] is employed due to its simplicity, stability and potential for power minimization with the gain provided by a single transistor. Fig. 3 illustrates the diagram of the Pierce oscillator for the extracted RLC tank as shown in Fig. 2(b) with the design approach adapted from previous work on low-power crystal oscillators [30]. An automatic gain control (AGC) circuit [11, 31] is added to minimize the power consumption by setting the transconductance, g_m, at the critical point. The AGC circuitry also helps prevent driving the MEMS resonator into the non-linear regime. The oscillator consumes less than 1µA (no load) from a 1.2-V supply.

B. Temperature Sensitivity

An important issue that needs to be addressed is that associated with the temperature sensitivity of the resonant frequency of the device [32]. This temperature sensitivity is normally associated with the variation of the Young's Modulus of single-crystal silicon with temperature. In a strain sensor application, where a silicon structure should be bonded onto the package carrier using an adhesive the overall temperature sensitivity can be influenced by additional factors as well. The change in temperature not only results in a variation in the elastic properties of the resonator structure (typical associated temperature coefficient of frequency, TCF, of approximately–26ppm/ºC to -30ppm/ºC), but the thermal expansion (or contraction) of the die, package carrier and adhesion layer also contributes to additional axial stress on the resonator. Changes in stress induced with temperature dependence on the resonator geometry, die and packaging carrier and must be considered on a case-by-case basis [27].

To evaluate the effect of temperature induced-stress, the behavior of two packaged prototypes were characterized with respect to temperature. These results are shown in Fig. 4. It is observed that in the case no adhesion is used the TCF is -27ppm/ºC compared to that of -34ppm/ºC for the case where the MEMS die is fully covered with 2-part epoxy adhesive (LOCTITE 3430). It is shown that the thermal stresses from the beam, carrier, adhesive layers contribute about -7ppm/ºC (or about 1.3Hz/ºC) to the measured resonance frequency. This value is subject to change if the device is attached onto another structure. For this reason, passive temperature compensation methods previously developed for MEMS resonators [21-23, 25] are not sufficient to compensate for temperature sensitivity as these usually address temperature sensitivity to material properties and device dimensions only. The following section will describe the dual resonator approach further in order to address this issue.

III. DUAL RESONATOR APPROACH FOR TEMPERATURE COMPENSATION

A SEM image of the dual resonator structure is shown in Fig. 5. It consists of 2 identical resonators oriented perpendicular to each other. Fig. 5 shows the schematic of the MEMS strain sensor attached on to package and host structure using adhesive. Resonant frequencies of the sense, f_S, and reference, f_R, resonator can be expressed as:

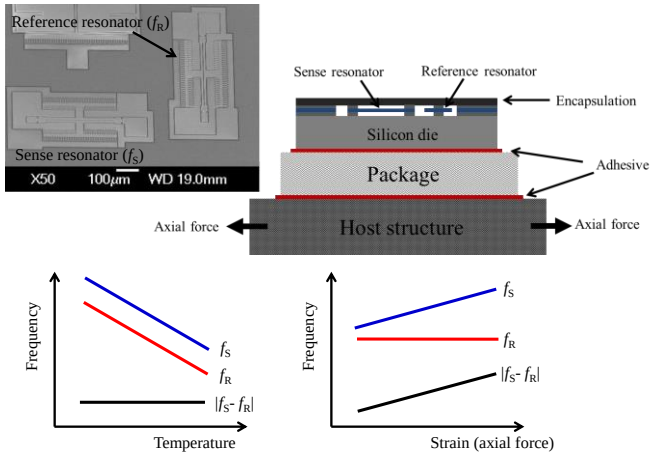

Fig. 5. Basic principle for first order temperature compensated strain sensor using dual-MEMS resonators.

$$f_S = f_{0S} + \alpha_1 \varepsilon + (TCF_{Si-S} + \beta_S)\Delta T \cdot f_{0S}$$
$$f_R = f_{0R} + \alpha_2 \varepsilon + (TCF_{Si-R} + \beta_R)\Delta T \cdot f_{0R} \quad (1)$$

where f_{0S} and f_{0R} are the resonant frequencies of the *sense* and *reference* resonators respectively for zero load at a particular temperature, ε is the strain induced on the attached sensor due to the mechanical deformation of the host structure to be monitored, α_1 is strain-frequency coefficient of the *sense* resonator, α_2 is strain-frequency coefficient of the *reference* resonator. TCF_{Si-S} and TCF_{Si-R} are temperature coefficients of frequency associated with changes in material properties and dimensions while β_S and β_R are thermal stress induced coefficients of several layers (including host structure, package, silicon die, adhesives) for the two resonators.

With the current design, if the DETF beam widths are mismatched by 1%, the frequency difference between f_{0S} and f_{0R} is estimated to be ~3kHz (1.5%). This mismatch will reduce the extent of temperature compensation achievable based on a reference resonator.

In practice, the resonant frequency of the two resonators can be matched ($f_{0S} = f_{0R} = f_0$) through design, post-fabrication or circuit level trimming. Single crystal silicon is an anisotropic material; however the directions of the two resonators are in the same crystal orientation {100} [33] for the wafer orientation adopted in this process. Therefore, the TCF factors are expected to be identical, $TCF_{Si-S} = TCF_{Si-R}$. As a result, by measuring the differential frequency between f_S and f_R, the TCF_{Si} could be cancelled as:

$$f_d = (\beta_S - \beta_R) f_0 \Delta T + (\alpha_1 - \alpha_2)\varepsilon \quad (2)$$

Furthermore, β_S and β_R can be potentially matched if isotropic materials are used for the adhesive, carrier and host structure. In this case, the differential frequency can be fully temperature compensated and expressed as:

$$f_d = (\alpha_1 - \alpha_2)\varepsilon \quad (3)$$

$\alpha_2 = 0$ in an ideal case, where the *reference* resonator is insensitive to the axial force.

Circuits that use a mixer and low-pass-filter to detect the frequency difference between two frequency sources are well established in previous literature. However, the challenge is in the realization of suitable topologies that simultaneously allow for high accuracy readout as well as low power dissipation.

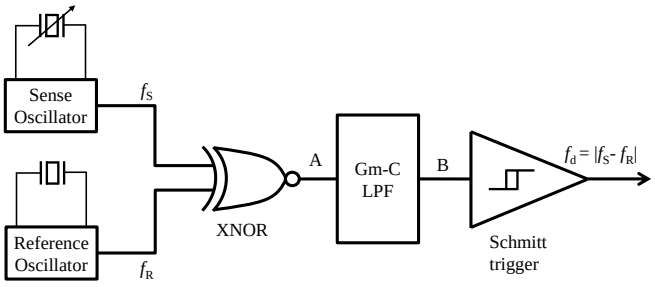

Fig. 6. Block diagram of the environmental effects compensation system for resonant sensors.

Furthermore, standard mixer topologies are best suited for sinusoidal inputs with square-wave and single-ended outputs resulting in additional implementation complexity [34]. Frequency subtractors which employ only one or two D-type flip-flops have been previously presented [35]; however, the signal output is very susceptible to jitter especially when the two input signals are in phase. To eliminate the resulting jitter further circuit complexity is necessary [36], often at the expense of additional power and the requirement for an additional reference clock.

Fig. 6 shows the block diagram of the circuit topology implemented for differential frequency detection. The square-wave output signals of both resonator-based oscillators are fed into the digital mixer implemented by a XNOR gate. The output of the XNOR is low if the two inputs to the gate are at different levels (one low and the other one is high), and high whenever the voltages of both inputs are equal. In other words, the frequency output A, of the XNOR gate consists of the difference and sum frequencies $|f_S - f_R|$ and $(f_S + f_R)$. In the next stage, the signal is fed into the Gm-C filter to suppress the high frequency component of the XNOR output. The cut-off frequency of Gm-C low-pass filter [37] is designed to fulfill this requirement while optimizing the power consumption of the circuit.

IV. Measurement Results

A CMOS oscillator and active compensation circuit are designed and fabricated in a standard 0.35 μm CMOS process. The MEMS chip, packaged within a metal base carrier module with CMOS circuitry, was attached to the test beam of a strain calibration apparatus using 2-part epoxy adhesive (LOCTITE 3430) as shown in Fig. 7. The thickness of the aluminium test beam is, h = 5mm. The deflection of the beam is varied and measured by a micrometer gauge, hence the strain of the test beam at the location of the MEMS device can be extrapolated [38]. The resulting axial strain on the DETF induces a shift in its resonant frequency and this is reflected in the frequency output of the feedback oscillator. Thus, the shift in the resonant frequency as a function of induced axial loading on

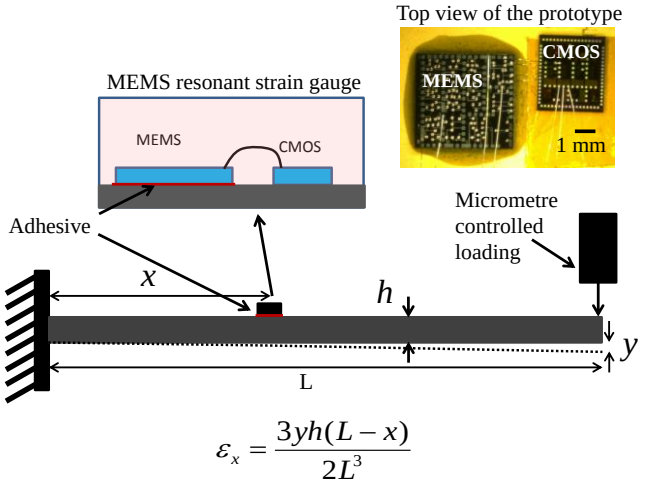

Fig. 7. Schematic of the strain calibration apparatus for the developed prototype.

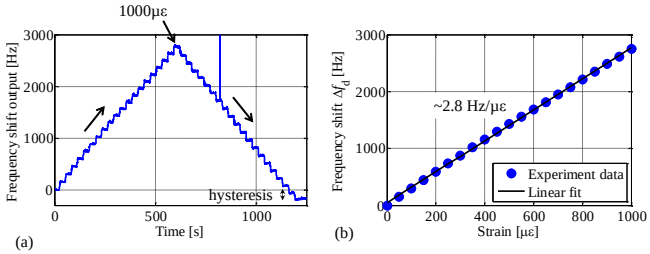

Fig. 8. Frequency-strain characterization of the MEMS resonant strain sensor. (a) Strain increased in 20 steps and released in 20 steps with 50με per step. (b) Extracted results for the strain ramp up.

the tuning fork can be monitored and characterized.

A DC bias voltage of 18V is employed as the polarization voltage for both resonators. The CMOS circuit can be operated at power supply voltages varying from 1V to 3.3V. The power consumption for the system is measured as 2.5μA for a 1.2V supply voltage. Due to fabrication tolerances in the manufacturing process, f_d is observed to be around 1.1kHz at room temperature (22ºC). The frequency split between the oscillators is ~0.6% (or 6000ppm) of the DETF center frequency of ~182kHz, which could be translated as DETF beam widths mismatched by ~0.4%.

Fig. 8 shows the characterized relationship between the output frequency and the strain using the strain calibration apparatus shown in Fig. 7. The scale factor of the device is seen to be approximately 2.8Hz/με. The scale factor is dependent on the device topology, material and thickness of the carrier as well as the adhesion layers [39, 40]. The sensor has been tested to a strain range of 1000με without damage to the package and encapsulated die demonstrating a linear coefficient of determination R^2 = 0.99 over this range. The ramp tests demonstrate a hysteresis of ~150Hz after the stress is released.

A second prototype device with no epoxy adhesive has been characterized to test the effectiveness of the temperature compensation between stress-induced and non-stress-induced effects. Allan deviations showing the stability of the two developed prototypes are plotted in Fig. 9. Both prototypes achieve similar level of stability though slight variations in performance can be seen. A minimum oscillator Allan deviation of 2.5mHz is recorded for an integration time of 10s

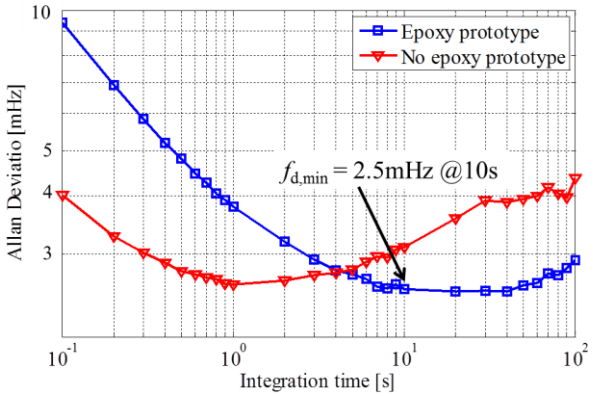

Fig. 9. Allan Deviation of the frequency output for two device prototypes at room temperature.

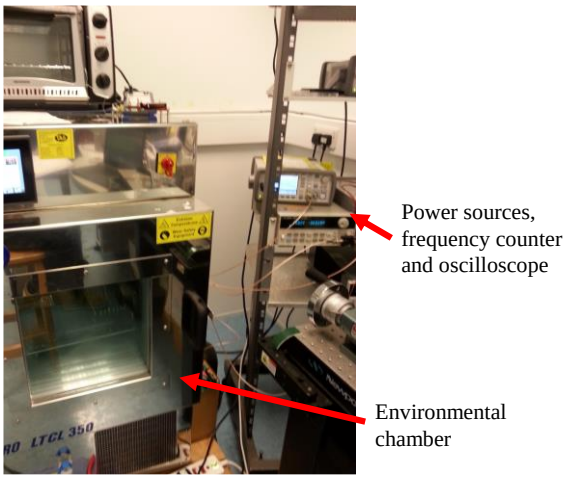

Fig. 10. Temperature sensitivity test setup.

on the prototype using the epoxy adhesive, corresponding to a minimum detectable strain of 9nε.

Temperature sensitivity experiments were carried out on two prototypes in an environmental chamber as shown in Fig. 10. Signal outputs of f_S, f_R and f_d are recorded using frequency counters (Agilent 53132A) or an oscilloscope. In the first prototype, Fig.11, where the MEMS die is isolated from the thermal stresses from carrier and host structure, the TCFs of both resonators are identical at around -5.2Hz/ºC. Consequently, the temperature effect on the detected differential frequency at the output of the system, f_d, is very small at ~0.022Hz/ºC. This translates to a value of ~20ppm/ºC for f_d, which is consistent with equation (2). It should be noted that f_d varies by only 1.7Hz over the temperature range from 22ºC to 85ºC. This variation can be minimized by improving the matching between the two resonators.

Fig. 12 shows the experimental results of the second prototype using the strain sensing setup with the MEMS die attached on to a metal base carrier module and the 5mm aluminum beam as shown in Fig. 5(b). Due to stress induced

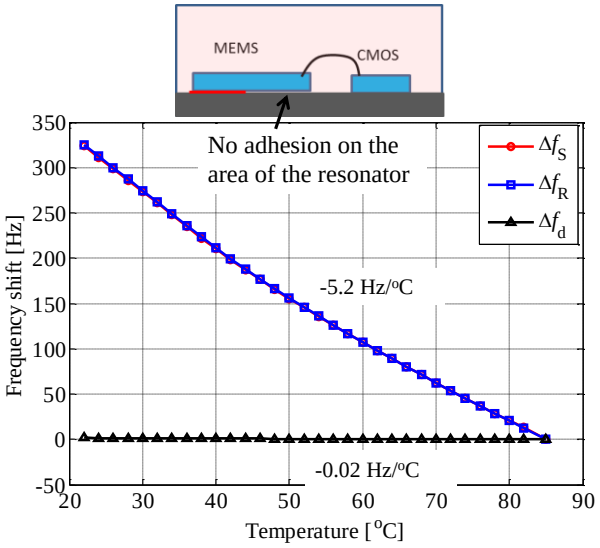

Fig. 11. Temperature compensation experiment of the dual resonator system with no stresses induced from carrier and host structure.

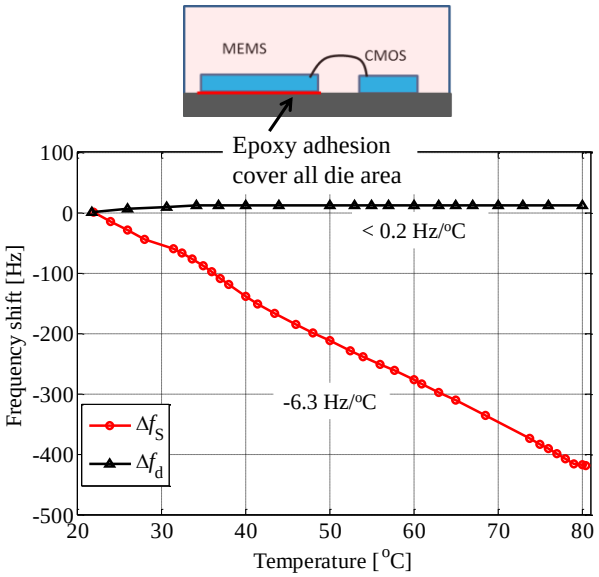

Fig. 12. Temperature compensation experiment of the dual resonator system under stresses induced from carrier and test beam.

from packaging, the TCFs of both resonators track each other and are increased to approximately -34ppm/°C (or -6.3Hz/°C). The TCF of the differential frequency, f_d, is reduced by 96% compared with the TCF of the resonator down to about 0.2Hz/°C over the range from 22°C to 80°C. This translates to a maximum error over temperature of 12Hz (or 4.3με) in the sensor output over the 58°C temperature range.

Table II compares this work to other state of the art MEMS-based, piezoelectric based strain sensors and commercial resistive strain gauges in terms of power, sensitivity and temperature compensation, demonstrating a substantial improvement over the current state-of-the art in term of power consumption and stress-induced temperature cancellation.

V. Discussion

The resonator design in this work is based on a double-ended tuning fork topology similar to designs reported in previous work [7-11, 17-19, 24, 26] with slightly lower resonant frequency (~187kHz versus ~215kHz). The scale factor of the device reported in this work is smaller at 2.8Hz/με compared to that reported previously reported with the difference potentially explained by the package and carrier used here as compared to previous work where the MEMS die is bonded directly onto the host structure. Maximizing sensitivity could be addressed by reducing the thickness of the package and the silicon die (which is 380μm in the current process); however the lower scale factor also allows for a large dynamic range with improved linearity relative to more sensitive prototypes. .

The interface circuit was tested with power supply voltage varying from 1V to 3.3V without significant variation in the output frequency. It should be noted that the stability of the DC polarization voltage is essential to ensure long-term stability of the sensor [29], hence a stable stand-alone DC source is recommended for applications demanding excellent long-term stability.

The device was cycled twice over temperature (22-80°C) and the scale-factor remained unchanged for this experiment. A similar prototype was subject to cyclic loading over a range from 10με to 500με and was found to be functional after 90000 cycles of loading though the scale-factor was found to have reduced by 17% after this test. This reduction might be due to the degradation of adhesion layer(s) or the resonator(s). Further systematic temperature and dynamic loading tests are warranted to elucidate the physical mechanisms underlying these observations and identify solutions to address these issues.

An appropriate calibration scheme must be developed for any misalignment in orientation of the *sense* resonator with respect to the direction of the applied stress. In case of misalignment, the scale factor for the *sense* resonant frequency will be reduced (α_1 decreased compared with the matched case), whereas the *reference* resonator is also subject to loading ($\alpha_2 > 0$), and hence its frequency also changes in proportion to the degree of angular misalignment. These issues can be addressed through the development of appropriate packaging schemes and the design of the host structure to ensure that the extent of angular misalignment is limited.

The hysteresis after strain release is possibly contributed due to improper package and adhesive materials used and/or related handling issues. Further work is underway to find an improved adhesive, e.g. solder paste [40], packaging material, e.g. alloy metal, and handling method to reduce the observed hysteresis in the response.

In applications where strains from both mechanical and thermal sources are of interest, the frequency output of both the sense and reference resonator could be monitored to provide readings for frequency and temperature simultaneously. An appropriate model would then have to be developed to infer the separate strain terms associated with mechanical and thermal sources and this could be developed through a purpose designed calibration scheme.

Further, in order to address practical applications to structural health monitoring a number of additional factors must be considered with regard to address full system integration and deployment. In a wireless sensor node, the sensor is likely to be integrated with a low-power microcontroller and this will enable implementation of appropriate frequency counting techniques required to digitize the signal output [10].

VI. Summary and Future Work

In this paper, a technical approach for the realization of a temperature compensated low-power vacuum packaged MEMS strain sensor is presented. The MEMS devices are fabricated in a foundry process and are vacuum encapsulated using a wafer-level packaging scheme. A dual resonator circuit readout scheme with differential frequency detection is implemented in a standard 0.35µm CMOS process to reduce the temperature sensitivity of the output response.

A vacuum packaged MEMS strain sensor prototype demonstrated a scale factor of 2.8Hz/µε over a measurement range up to 1000µε. The temperature sensitivity of the device is reduced to 0.2Hz/ºC from 6.3Hz/ºC over the temperature range from 22ºC to 80ºC. The power consumption of 3 microwatts makes this device an excellent candidate for many applications especially battery-powered or energy harvesting enabled applications.

It is seen that limits to temperature compensation arise from the matching of the thermal stresses induced by the adhesive and package and the relatively simple compensation scheme employed. Ongoing research is addressing improved approaches for device packaging to more substantially compensate temperature variations as well as to reduce the hysteresis in response due to stress relaxation (in the adhesive) following cyclic loading on the device. An on-chip DC bias generator based on a charge pump circuit [43] is being developed to eliminate the cumbersome high voltage batteries at the expense of some increase in power consumption [44]. Integration of the MEMS strain sensor into a wireless sensor network for infrastructure monitoring is also being pursued.

Acknowledgments

This work was supported by the UK Engineering and Physical Sciences Research Council (Grant EP/K000314/1) and the Cambridge Centre for Smart Infrastructure and Construction. The authors would like to thank Dr Alberto Roncaglia (CNR Italy) and Dr Luca Belsito (CNR Italy) for helpful discussions.

References

[1] J P. Lynch, and K. J. Loh, "A summary review of wireless sensors and sensor networks for structural health monitoring." *Shock and Vibration Digest*, vol. 38, no. 2, pp. 91-128, 2006.

[2] T. Torfs *et al.*, "Low power wireless sensor network for building monitoring", *IEEE Sensors Journal*, vol. 13, no. 3, pp. 909-915, 2013.

[3] C. L. Roozeboom *et al.*, "Multifunctional Integrated Sensors for Multiparameter Monitoring Applications", *J. Microelectromech. Syst*., vol. 24, no. 4, pp. 810–820, 2015.

[4] K. Brueckner *et al.*, "Micro-and nano-electromechanical resonators based on SiC and group III-nitrides for sensor applications." *physica status solidi*, vol. 208, no. 2, pp. 357-376, 2011.

[5] T. Nagayama, M. Ruiz-Sandoval, B. F. Spencer, K. A. Mechitov, and G. Agha, "Wireless strain sensor development for civil infrastructure." In *Proceedings of First International Workshop on Networked Sensing Systems*, vol. 5, 2004.

[6] Y. Jia, C. D. Do, X. Zou and A. A. Seshia, "A Hybrid Vibration Powered Microelectromechanical Strain Gauge" *IEEE Sensors Journal*, vol. 16, no. 1, pp. 235-241, 2016.

[7] A. A. Seshia, M. Palaniapan, T. A. Roessig, R. T. Howe, R. W. Gooch, T. R. Schimert, and S. Montague, "A vacuum packaged surface micromachined resonant accelerometer," *J. Microelectromech. Syst*., vol. 11, no. 6, pp. 784–793, 2002.

[8] M. Ferri, F. Mancarella, L. Belsito, A. Roncaglia, J. Yan, A. A. Seshia, K. Soga, and J. Zalesky, "Strain sensing on steel surfaces using vacuum packaged MEMS resonators." *Procedia Engineering*, vol. 5 pp. 1426-1429, 2010.

[9] L. Belsito, M. Ferri, F. Mancarella, A. Roncaglia, J. Yan, A. A. Seshia, and K. Soga, "High resolution strain sensing on steel by silicon-on-insulator flexural resonators fabricated with chip-level vacuum packaging" in *Transducers*, Barcelona, Spain, 16-20 June 2013.

[10] L. Belsito, M. Ferri, F. Mancarella, L. Masini, J. Yan, A. A. Seshia, K. Soga and A. Roncaglia, Fabrication of high-resolution strain sensors based on wafer-level vacuum packaged MEMS resonators, *Sensors and Actuators A: Physical*, Vol. 239, pp. 90-101, 2016.

[11] C. Do, A. Erbes, J. Yan, and A. Seshia, "Low power mems oscillators for sensor applications," in *Digest Tech. Papers EFTF*, Neuchatel, June 2014.

[12] G. R. Witt, "The electromechanical properties of thin films and the thin film strain gauge," in *Thin Solid Films*, vol. 22, pp. 133-156, 1974.

[13] P. J. French and A. G. R. Evans, "Piezoresistance in polysilicon and its applications to strain gauges," in *Solid-State Electronics*, vol. 32, no. 1, pp. 1-10, 1989.

[14] E. EerNisse, "Miniature quartz resonator force transducer," U.S. Patent 4215570A, 1980.

[15] E. P. EerNisse, R. W. Ward and R. B. Wiggins, "Survey of quartz bulk resonator sensor technologies," in *IEEE Trans. Ultrason. Ferroelectr. Freq. Control*, vol. 35, no. 3, pp. 323-330, 1988.

[16] H. A. C. Tilmans, M. Elwenspoek, and J. H. J. Fluitman, "Micro resonant force gauges." *Sensors and Actuators A: Physical*, vol.30, no. 1-2, pp 35-53, 1992.

[17] S. P. Beeby, G. Ensell, B. R. Baker, M. J. Tudor, and N. M. White, "Micromachined silicon resonant strain gauges fabricated using SOI wafer technology." *J. Microelectromech. Syst.*, no. 1, pp. 104-111, 2000.

[18] K. E. Wojciechowski, B. E. Boser, and A. P. Pisano. "A MEMS

TABLE II
PERFORMANCE COMPARISON WITH STATE-OF-THE ART MEMS STRAIN SENSOR AND COMMERCIAL RESISTIVE STRAIN GAUGE

Parameters	[5] 4.5kΩ gauge	[41] MEMS capacitive	[42] Piezoelectric	[9] MEMS resonator	[This work] MEMS resonator
Readout circuit	PCB	1.5µm CMOS	PCB	PCB	0.35µm CMOS
Power	>2mA@±5V*	1.5mA@3V[a]	>2mA@±5V*	~100mA@±5V*	2.5µA@1.2V
Scale factor	NA	816 µV/µε	340µV/µε	120Hz/ µε	2.8Hz/µε
Sensitivity	4µε	0.87µε	28.7nε	4nε	9nε
Range (µε)	>±2000	±1000	NA	±2.5	1000
Stress-induced cancellation	Yes	No	No	No	Yes

* Estimation based on ±5V supply on instrumentation amplifier used.

[a] Power of CMOS readout circuit, not including RF circuitry

resonant strain sensor operated in air." *In Micro Electro Mechanical Systems, 17th IEEE International Conference on.(MEMS)*, pp. 841-845, 2004.
[19] R. G. Azevedo, D. G. Jones, A. V. Jog, B. Jamshidi, D. R. Myers, L. Chen, X. Fu, M. Mehregany, M. Wijesundara, and A. P. Pisano, "A SiC MEMS resonant strain sensor for harsh environment applications." *IEEE Sensors Journal*, vol. 7, no. 4, pp. 568-576, 2007.
[20] H. A. C. Tilmans, S. Bouwstra, D. J. IJntema, M. Elwenspoek, and C. F. Klein. "A differential resonator design using a bossed structure for applications in mechanical sensors." *Sensors and Actuators A: Physical*, vol. 26, no. 1, pp. 385-393, 1991.
[21] K. Sundaresan, G. K. Ho, S. Pourkamali, and F. Ayazi, "Electronically temperature compensated silicon bulk acoustic resonator reference oscillators," *IEEE J. Solid-State Circuits*, vol. 42, pp. 1425-1434, 2007.
[22] M. Hopcroft, R. Melamud, R. N. Candler, W.-T. Park, B. Kim, G. Yama, A. Partridge, M. Lutz, and T. W. Kenny, "Active temperature compensation for micromachined resonators," in *Solid-State Sensor, Actuator and Microsystems Workshop*, Hilton Head Island, South Carolina, pp. 364-367, 2004.
[23] W.-T. Hsu and C. T. C. Nguyen, "Geometric stress compensation for enhanced thermal stability in micromechanical resonators," in *Ultrasonics Symposium, Proceedings, IEEE*, pp. 945-948, 1998.
[24] D. R. Myers, R. G. Azevedo, L. Chen, M. Mehregany, and A. P. Pisano, "Passive substrate temperature compensation of doubly anchored double-ended tuning forks." *J. Microelectromech. Syst.*, vol. 21, no. 6, pp. 1321-1328, 2012.
[25] A. K. Samarao and F. Ayazi, "Temperature compensation of silicon resonators via degenerate doping," *Electron Devices, IEEE Transactions on*, vol. 59, no. 1, pp. 87-93, 2012.
[26] R. G. Azevedo, W. Huang, O. M. O'Reilly, and A. P. Pisano, "Dual-mode temperature compensation for a comb-driven MEMS resonant strain gauge." *Sensors and Actuators A: Physical*, vol. 144, no. 2, pp. 374-380, 2008.
[27] R. Melamud, M. Hopcroft, C. Jha, B. Kim, S. Chandorkar, R. Candler, and T. W. Kenny, "Effects of stress on the temperature coefficient of frequency in double clamped resonators." In *Solid-State Sensors, Actuators and Microsystems, The 13th International Conference on (Transducer)*, 2005.
[28] J. E-Y. Lee, B. Bahreyni, and A. A. Seshia, An axial strain modulated double-ended tuning fork electrometer, *Sensors and Actuators, Part A: Physical*, Vol. 148, No. 2, pp. 395-400, December 2008.
[29] C.T-C. Nguyen and R. T. Howe, "An integrated CMOS micromechanical resonator high-Q oscillator," *IEEE J. Solid-State Circuits*, vol. 34, pp. 440-455, 1999.
[30] E. Vittoz, M. G. R. Degrauwe, S. Bitz, "High-performance crystal oscillator circuits: theory and application", *IEEE J. Solid-State Circuits*, vol. 23, no. 3, pp. 774-783, Jun.1988.
[31] E. Vittoz and J. Fellrath, "CMOS analog circuits based on weak inversion operation," *IEEE J. Solid-State Circuits*, vol. SC-12, pp.224–231, June 1977.
[32] C.T-C. Nguyen, "MEMS technology for timing and frequency control." *Ultrasonics, Ferroelectrics, and Frequency Control, IEEE Transactions on* 54, no. 2, pp. 251-270, 2007.
[33] M. Hopcroft, W. D. Nix, and T. W. Kenny, "What is the Young's Modulus of Silicon?." *J. Microelectromech. Syst*., vol. 19, no. 2, pp. 229-238, 2010.
[34] B. Razavi, RF microelectronics, 2nd Edition, New Jersey, Prentice Hall, 2012
[35] R. Javeri, Frequency subtractor, U.S. Patent No. 4,683,437, 1987.
[36] J. P. Norris, Apparatus for detecting a frequency deviation between two frequency sources, U.S. Patent No. 5,313,154, 1994.
[37] R. L. Geiger and E. Sanchez-Sinencio, "Active filter design using operational transconductance amplifiers: a tutorial," *Circuits and Devices Magazine, IEEE*, vol. 1, pp. 20-32, 1985.
[38] J. M. Gere, S. P. Timoshenko, "Mechanics of Materials", Chap. 10, PWS Publishing Company, 1997.
[39] R. G. Azevedo, I. Chen, O. M. O'Reilly and A. P. Pisano, "Influence of Sensor Substrate Geometry on the Sensitivity of MEMS Micro-Extensometers," in *ASME International Mechanical Engineering Congress and Exposition*, Orlando, FL, pp. 307-312, 2005.
[40] B. D. Sosnowchik, R. G. Azevedo, D. R. Myers, M. D. Chan, A. P. Pisano and L. Lin, "Rapid Silicon-to-Steel Bonding by Induction Heating for MEMS Strain Sensors," *J. Microoelectromech. Syst.*, vol. 21, no. 2, pp. 497-506, 2012.
[41] M. Suster, et al., "A wireless strain sensing microsystem with external RF power source and two-channel data telemetry capability." ISSCC Dig. Tech. papers, Feb. 2007.
[42] S. Kon, R. Horowitz, "High-resolution MEMS piezoelectric strain sensor for structural vibration detection", *IEEE Sensor*, vol. 8, no. 12, pp. 2027-2035, 2008.
[43] M. D. Ker, S. L. Chen, C. S. Tsai, "Design of Charge Pump circuit with consideration of gate-oxide reliability in low-voltage CMOS process", *J. Solid-State Circuit*, vol. 41, no. 5, pp. 1100-1107, 2006.
[44] K. R. Cioffi and W. T. Su, "32KHz MEMS-based oscillator for low power application", *Freq. Control Sym. And Exp., Proceedings of the 2005 IEEE International*, p. 551-558, 2005

Cuong Do received B.Sc. in Electronics and Telecommunication from Vietnam National University, Hanoi in 2004, M.Eng. in Electronics from Chungbuk National University, Korea in 2007, and PhD in Electronics from Cork Institute of Technology, Ireland in 2012. He is now Research Associate in the University of Cambridge. His research focuses on both fields of MEMS and CMOS interface circuit for low-power sensor and timing applications.

Andreja Erbes received his MEng (2011), MA (2014) and Ph.D. (2015) in Electrical and Electronic Engineering from the Department of Engineering at the University of Cambridge. In 2009, he spent a year abroad at the Massachusetts Institute of Technology within the Cambridge-MIT Exchange Program and took part in an undergraduate-research opportunity program (UROP) within the Weinstein Research Group working in the field of Micro-Electro-Mechanical-Systems (MEMS). His research includes the design of MEMS resonators and CMOS circuits for low power wireless communications, timing applications and electrical interfacing of MEMS-based sensors.

Jize Yan received the first degree from Tsinghua University in China in 2003, and Ph.D. degree in 2007 from the University of Cambridge. He is now a Principal Investigator/Senior Research Associate in the University of Cambridge. His research has a focus on high-Q MEMS resonators in RF MEMS, MEMS sensor and Power MEMS. He also has strong research activities in wireless sensor network, distributed fibre optic sensors and power electronics for civil engineering and energy applications. His work led to 60+ peer-reviewed publications, 8 patents and several best paper awards. He has worked with 30+ industrial collaborators.

Kenichi Soga is Professor of Civil Engineering and the Head of the Geotechnical Group at the University of Cambridge. He is Fellow of the Royal Academy of Engineering and Fellow of

the Institution of Civil Engineers. He obtained his BEng and MEng from Kyoto University in Japan and PhD from the University of California at Berkeley in 1994. His current research activities are innovative monitoring and long-term performance of civil engineering infrastructure, energy geomechanics, and modelling of construction processes. He has published more than 300 journal and conference papers and is co-author of "Fundamentals of Soil Behavior, 3rd edition" with Professor James K Mitchell. He is recipient of many awards including George Stephenson Medal (2006) and Telford Gold Medal (2010) from the Institution of Civil Engineers and Walter L. Huber Civil Engineering Research Prize (2007) from the American Society of Civil Engineers. He is a founding member of the Cambridge Centre for Smart Infrastructure and Construction (CSIC).

Ashwin A. Seshia received his BTech in Engineering Physics in 1996 from IIT Bombay, MS and PhD degrees in Electrical Engineering and Computer Sciences from the University of California, Berkeley in 1999 and 2002 respectively, and the MA from the University of Cambridge in 2008. During his time at the University of California, Berkeley, he was affiliated with the Berkeley Sensor & Actuator Center. He joined the faculty of the Engineering Department at the University of Cambridge in October 2002 where he is presently a Reader in Microsystems Technology and a Fellow of Queens' College. He is a Fellow of the Institute of Physics, a Fellow of the Institution for Engineering and Technology and a senior member of the Institute of Electrical and Electronics Engineers. His research interests are in the domain of microengineered dynamical systems with applications to sensors and sensor systems. Dr Seshia serves on the editorial boards of the IEEE Journal of Microelectromechanical systems, IOP Journal of Micromechanics and Microengineering, IEEE Transactions on Nanotechnology and the IEEE Transactions on Ultrasonics, Ferroelectrics and Frequency Control.